ELSEVIER

Soil Dynamics and Earthquake Engineering 21 (2001) 275–286

SOIL DYNAMICS AND EARTHQUAKE ENGINEERING

www.elsevier.com/locate/soildyn

A note on the useable dynamic range of accelerographs recording translation[1]

M.D. Trifunac*, M.I. Todorovska

Civil Engineering Department, University of Southern California, Los Angeles, CA 90089-2531, USA

Accepted 11 February 2001

Abstract

Since the late 1970s, the dynamic range and resolution of strong motion digital recorders have leaped from 65 to 135 dB, opening new possibilities for advanced data processing and interpretation. One of these new possibilities is the calculation of permanent displacement of the ground or of structures, associated with faulting or with non-linear response. Proposals on how permanent displacements could be recovered from recorded strong motion have been published since 1976. The analysis in this paper concludes that permanent displacements of the ground and of structures in the near-field can be calculated provided all six components of strong motion (three translations and three rotations) have been recorded, and the records are corrected for transducer rotation, misalignment and cross-axis sensitivity.

Keywords: Strong motion recording; Strong motion data processing; Digitization noise; Permanent displacement; Rotational components of strong motion; Strong motion transducers

1. Introduction

One of the oldest challenges in strong motion measurements has been the computation of velocity and displacement from recorded accelerograms, mostly due to the fact that the zero baseline of the recorded acceleration is not known. Prior to the first studies of digitization noise [1], the majority of investigators assumed the zero baseline to be of parabolic form. Starting in the late 1960s and early 1970s, a new baseline correction procedure was introduced, essentially as a by-product of filtering out the recording, digitization and processing noise below a suitably chosen frequency where the signal to noise ratio approaches unity [2–4]. For the past 30 years, virtually all the analog strong motion data in the world have been processed following these procedures. Comparisons of computed and 'recorded' displacements have shown that this approach produces very accurate and stable estimates of the true ground velocity and displacements [5], but only within a limited frequency band, typically between 0.1 and 25 Hz [6,7]. Consequently, computation of permanent displacement (i.e. displacement at zero frequency) from such data is impossible.

The first three-dimensional high frequency inversion studies of the earthquake source [8,9], that followed the pioneering formulation of a kinematic earthquake source model by Haskell [10], demonstrated a need to compute permanent ground displacements from recorded strong motion accelerograms. A proposal on how to perform baseline correction that would allow estimation of permanent displacements 'when the influence of turning and inclination may be neglected' was made by Bogdanov and Graizer [11]. On the basis of shaking table experiments (involving one-dimensional translation only), it was estimated [12] that this new algorithm can compute permanent displacements with accuracy better than 25%, when the signal to noise ratio exceeds 50 (34 dB).

The resolution and dynamic range of strong motion accelerographs did not change much between 1930 and 1980, and was in the range 45–55 dB for most paper and film recording analog instruments. Between 1975 and 1980, with the rapid developments in solid-state technology, digital strong motion accelerographs began to appear [13]. This resulted in rapid growth of both resolution and dynamic range of strong motion accelerographs, which at

* Corresponding author. Tel.: +1-213-740-0570; fax: +1-213-744-1426.
E-mail address: trifunac@usc.edu (M.D. Trifunac).

[1] We dedicate this paper to Donald E. Hudson (1916–1999), a pioneer in the field of Earthquake Engineering, and our teacher and mentor. His contributions to academic research and development of earthquake instrumentation are without parallel. With a rare ability to attract, motivate and support young scientists, he created a long and impressive list of PhD graduates who are now professors, researchers and leaders in Earthquake Engineering.

0267-7261/01/$ - see front matter
PII: S0267-7261(01)00014-8

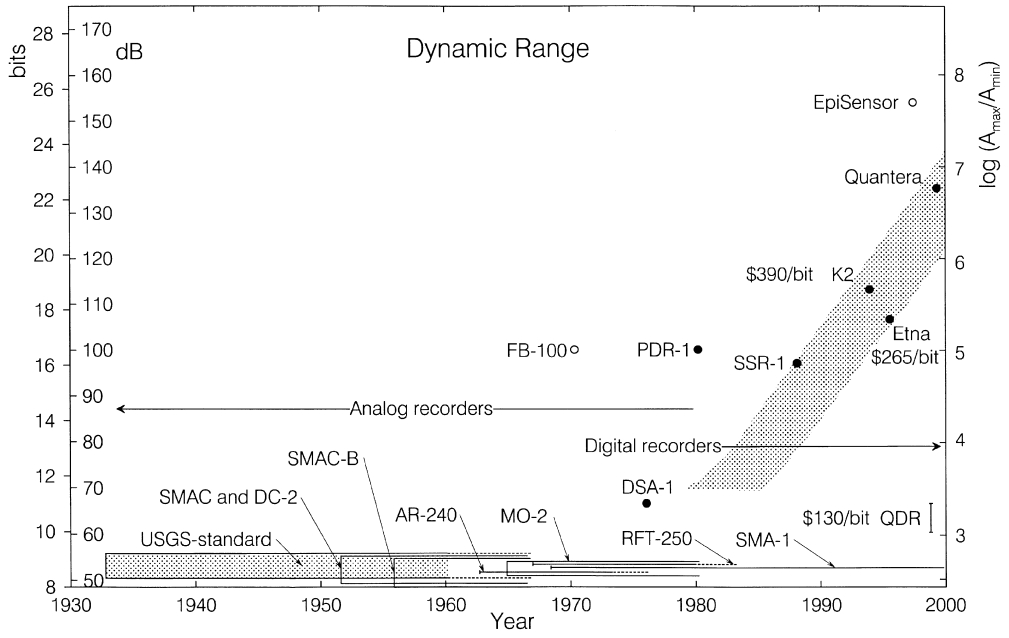

Fig. 1. Dynamic range (dB), resolution (bits) and log (A_{max}/A_{min}) of selected strong motion accelerographs and digital recorders from 1930 to 2000, and the dynamic range of two transducers (FBA-100 and EpiSensor) [13].

present are close to 135 dB (Fig. 1). One of the motives for this ever-increasing dynamic range has been the desire to compute permanent ground displacements, since 'digital instruments could be used to extract significantly more information about the displacement than the analog instruments' [14]. This has created a dangerous circulus viciosus, in which the low amplitudes of recording noise alone have been taken implicitly as the only required condition for computing permanent ground displacements, ignoring details of the physical nature of the problem, and without a careful analysis of what the strong motion transducers actually record [15,16].

This paper addresses the physical constraints in integration of recorded accelerograms and definition of zero-acceleration baseline, and the completeness of the forcing function in modeling strong motion transducers. The complete forcing function includes terms related to tilting and torsion of the instrument housing, transducer cross-axis sensitivity (i.e. recording components of motion in directions other than the principal sensitivity axis) and transducer misalignment (i.e. the angles between the transducers recording three components of motion are not exactly 90°) in addition to the principal driving forces represented by translational acceleration. The contributions from tilting and torsion are illustrated using artificially generated rocking and torsional ground motion time histories. The conclusion reached is that, to compute permanent ground displacement, it is necessary to record all six components of ground motion (three translations and three rotations). This was stated earlier by Graizer [17], but with less detailed quantification of the contributions from the rotational components of motion.

2. Model

2.1. Equations of motion of strong motion transducers

Many strong motion transducers are (or are equivalent to) penduli that rotate due to acceleration of their supports. Their motion is recorded by deflecting a light beam projected onto paper or film [18–22], by induction of voltage in a coil moving in a permanent magnetic field, by recording the current in a coil proportional to the inertial force of the transducer mass, or by measuring relative displacement via variable capacitance [23,24]. Fig. 2 shows an example of a viscously damped (by a moving coil in a magnetic field) pendulum transducer used in SMA-1 strong motion accelerograph [25]. The arm of the pendulum is designated by r. The sensitivity axis and the axis of rotation of the pendulum are also shown. The mutual placement and relative orientation of the transducer penduli with respect to the longitudinal (L), transverse (T) and vertical (V) axes of a SMA-1 accelerograph are shown in Figs. 3 and 4, where X_1, X_2 and X_3 are respectively displacements positive in the directions opposite of the L, T and V axes, and ϕ_i is a rotation about the X_i axis. For small deflections $y_i = r_i\alpha_i$, where α_i is the angle of deflection of the ith pendulum from its equilibrium position, the equations of motion of the penduli are: [17]

$$L:\ \ddot{y}_1 + 2\omega_1\zeta_1\dot{y}_1 + \omega_1^2 y_1 = -\ddot{X}_1 + \phi_2 g - \ddot{\phi}_3 r_1 + \ddot{X}_2\alpha_1 \tag{1a}$$

$$T:\ \ddot{y}_2 + 2\omega_2\zeta_2\dot{y}_2 + \omega_2^2 y_2 = -\ddot{X}_2 - \phi_1 g + \ddot{\phi}_3 r_2 + \ddot{X}_1\alpha_2 \tag{1b}$$

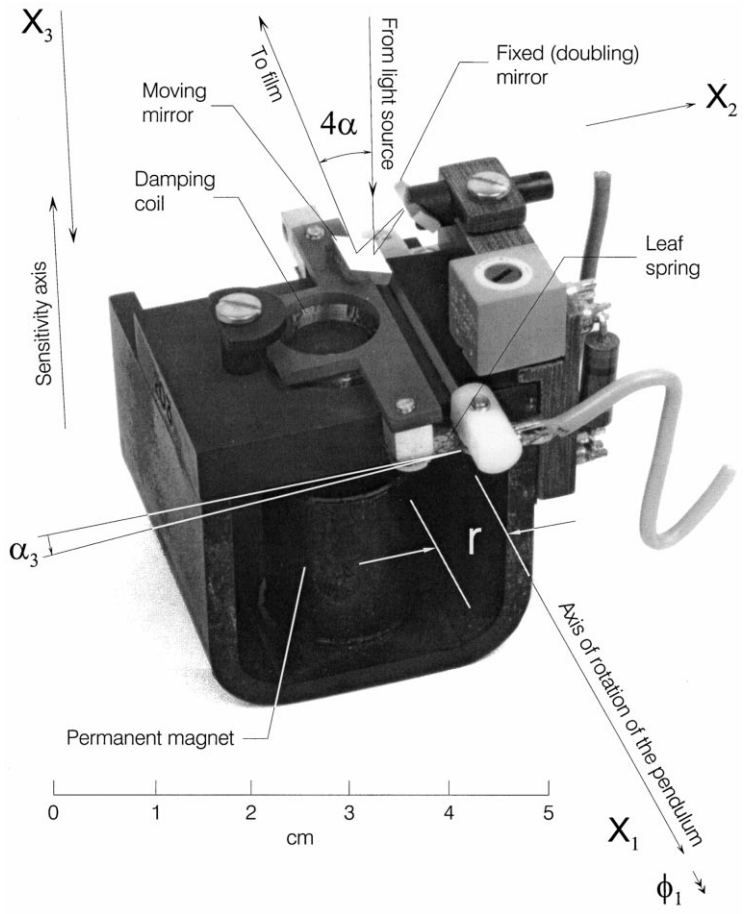

Fig. 2. An SMA-1 transducer removed from the box. Letter *r* indicates the arm of the pendulum and α is the angle of deflection. A double reflection of the light beam from the mirror attached to the pendulum creates rotation of the light beam by 4α. The coordinate axes X_1, X_2 and X_3 and angles of rotation α_3 and ϕ_1 are such as to illustrate configuration of a transducer sensitive to vertical motion.

$$V:\ \ddot{y}_3 + 2\omega_3\zeta_3\dot{y}_3 + \omega_3^2 y_3 = -\ddot{X}_3 - \ddot{\phi}_1 r_3 - \ddot{X}_2\alpha_3 \qquad (1c)$$

where ω_i and ζ_i are respectively the natural frequency and fraction of critical damping of the *i*th transducer. The second and third terms on the right hand side of Eqs. (1a) and (b) represent contributions from titling (ϕ_1 and ϕ_2) and angular acceleration ($\ddot{\phi}_3$) to the recorded responses y_1 and y_2. The tilting of the instrument does not contribute to the linearized equation for y_3 (Eq. 1c), but the angular acceleration $\ddot{\phi}_1$ does. The last terms on the right hand side in all three equations represent the contribution to the response from cross-axis sensitivity [25,26].

In typical computation of translational velocities ($\dot{X}_i$) and displacements (X_i) from recorded accelerograms, the contributions of all terms on the right-hand side of Eq. (1) (i.e. the forcing function terms) except $\ddot{X}_i$ are neglected. This is justified as long as the Fourier spectrum amplitudes of the neglected terms are smaller than those of the recording, digitization and processing noise combined. Regrettably, as Graizer [27] pointed out, the completeness of representing Eq. (1) in literature varies. For example, Golitsyn [19] does not take into account the cross-axis sensitivity, while Aki and Richards [28] ignore the angular acceleration terms.

Eq. (1) is representative of most strong motion transducers. For some, the cross-axis sensitivity terms $\ddot{X}_i\alpha_j$ may be negligible, while for others $r_i = 0$. The terms caused by the tilting $\phi_i g$ are always present and cannot be neglected.

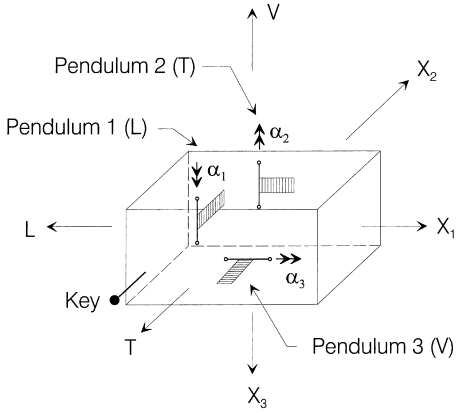

Fig. 3. Schematic representation of three transducers in a SMA-1 accelerograph. The coordinate axes X_1, X_2 and X_3 serve to describe the motion of the *L*, *T* and *V* transducers respectively, and are oriented in the opposite direction of the sensitivity axes of the transducers. Angles α_1, α_2 and α_3 describe the deflection of the transducer perduli.

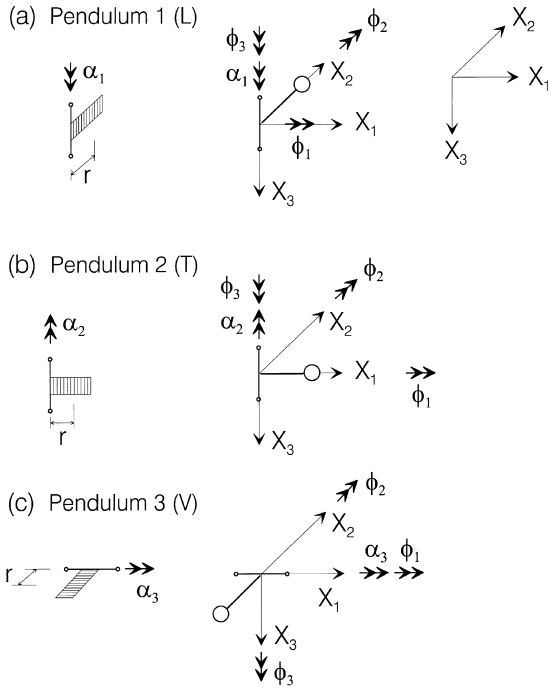

Fig. 4. Deflection angels of transducer penduli α_1, α_2 and α_3, rotation components of ground motion ϕ_1, ϕ_2 and ϕ_3 (shown by double arrows), and translational components of ground motion X_1, X_2 and X_3.

2.2. Computation of permanent displacements

The first attempt to compute permanent ground displacement from recorded strong motion accelerograms appears to have been by Bogdanov and Graizer [11]. They started with the following equation relating the recorded amplitudes $\ddot{y}(t)$ to the ground displacement $X(t)$

$$\ddot{y} + 2\omega_n\zeta\dot{y} + \omega_n^2 y = -V_0\ddot{X} \tag{2}$$

where ω_n and ζ are the natural frequency and fraction of critical damping in the recording transducer and V_0 represents a magnification factor. They proposed to determine the acceleration baseline as a polynomial (at first of a third degree and later of higher degrees) by minimizing the functional

$$W = \int_0^{T_1} [\dot{x}(t)]^2 \mathrm{d}t + \int_{T_2}^{T} [\dot{x}(t)]^2 \mathrm{d}t. \tag{3}$$

where T is the length of the recorded signal and T_1 and T_2 are times such that $0 < T_1 < T_2 < T$. This approach is based on the assumption that time intervals $[0, T_1]$ and $[T_2, T]$ can be found during which the ground motion is 'very small' compared to the strong motion amplitudes [27].

It appears this approach might work if: (1) the contributions from tilting and of angular accelerations to the recorded accelerogram are negligible, (2) the interval $[0, T_1]$ is such that T_1 occurs before the P-wave arrival (this obviously cannot be done for analog strong motion accelerographs which do not have pre-event memory) and (3) the interval $[T_2, T]$ is long compared to the long period surface and coda waves. Perusal of the work of Graizer and coworkers and of various more recent duplications of their idea do not reveal adequate information on actually chosen values of T_1, T_2 and T, and hence it is not possible to evaluate whether all or some of the above three requirements have been satisfied.

Trifunac and Lee adopted a more conservative approach, assuming that permanent ground displacements cannot be calculated from digitized analog records of translation only [4,5,29]. They worked with simplified Eq. (2) because the digitization noise in analog records is large. However they did consider other corrections associated with the governing Eq. (1) [24,30], cross axis sensitivity [26], and misalignment of transducer sensitivity axes [25,31].

2.3. Estimation of rotational components of strong motion from recorded translations

Instrumental data on rotational components of strong motion are rare [32,33], but there are some records on rotational strong motion in the proximity of explosions [34]. Measurement and interpretation of rotational components of strong motion is invaluable for high frequency source mechanism studies and for dynamic analyses of tall structures [35,36].

In the absence of recorded data, the nature of strong motion rotations can be studied if the wave content of strong motion is known, in particular its decomposition into the elementary constituents: P and S body waves, and Love and Rayleigh surface waves [37,38]. Then, for a given content of translational motion, the rotational components can be constructed using theoretical relationships between the complex amplitudes of translational and rotational wave motions for each of the constituents [39]. To simplify the work and without any loss of generality, the synthesis of rotational motion can be separated into two parts: one associated with pure shear, involving the contributions from SH and Love waves and resulting in torsional strong motion [40], and the other one associated with P, SV and Rayleigh waves and resulting in rocking strong motion [41]. For both decompositions, the spectra of translations, $A(\omega)$, and rotations $\psi(\omega)$ are related by:

$$\Psi(\omega) \approx A(\omega)a\omega/c(\omega) \tag{4}$$

where ω is frequency, $a = 1/2$ for torsion and $a = 1$ for rocking, and $c(\omega)$ is the phase velocity of a surface wave mode. Furthermore, $c(\omega) \to \beta_{\min}$ as $\omega \to \infty$ and $c(\omega) \to \beta_{\max}$ as $\omega \to 0$. For a layered half space, $\beta_{\min}$ and $\beta_{\max}$ are the smallest and the largest shear wave velocities in the medium. Between the two limits, $a\omega/c(\omega)$ changes slowly and monotonically, and log $\psi(\omega)$ versus log ω can be approximated by a straight line (see Fig. 9 in Lee and Trifunac [40]; and Figs. 12 and 13 in Lee and Trifunac [41]). In the right hand side of Eq. (4), the product $\omega\, A(\omega)$ is the Fourier spectrum of velocity; this implies that the Fourier

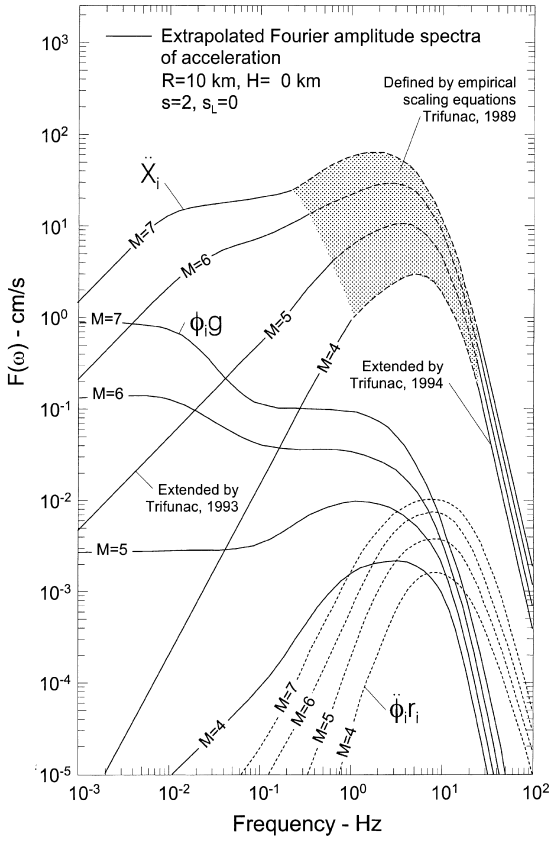

Fig. 5. Fourier amplitude spectra of ground acceleration, $\ddot{X}_i$, normalized rocking, $\phi_i g$, and normalized torsional acceleration, $\ddot{\phi}_i r_i$, at a site on basement rock ($s = 2$), and 'rock' soil condition ($s_L = 0$), for earthquake magnitudes $M = 4$, 5, 6 and 7, zero source depth and epicentral distance $R = 10$ km. The shaded region indicates the range where empirical scaling laws apply [42–44].

spectrum of rotations is proportional to the ratio between the Fourier spectrum of velocity and the phase velocity $c(\omega)$.

3. Illustrations

In this section, we illustrate the spectra of the forcing function terms in Eq. (1) that result from rocking and torsion of the instrument housing, and compare them with the spectra of translational motions, of digitization and recording noise, and with the threshold recording amplitudes of several strong motion accelerographs (recorders).

3.1. Estimates of $\phi_i g$ and $\ddot{\phi}_i r_i$ from scaling laws of translational spectra

Fig. 5 illustrates smooth Fourier amplitude spectra of strong motion acceleration, for epicentral distance $R = 10$ km, source at depth $H = 0$ km (surface fault), a site located on basement rock ($s = 2$) and on 'rock' soil ($s_L = 0$), and for 50% probability of exceedance (average spectra). The gray zone shows the range where the spectra can be defined by empirical scaling equations [42]. Extension of these spectra to high [43] and low [44] frequencies is possible, based on known scattering and attenuation properties of the medium at high frequencies, and on static (permanent) ground displacements on the fault surface in the limit when the frequency goes to zero. Fig. 5 shows that, for this example, $F(\omega) \sim \omega^2$ for $M = 4$ and for frequencies ($f = \omega/2\pi$) less than 1 Hz. As M increases, this slope decreases and for $M \geq 6$ a 'bulge' appears implying more long period energy associated with permanent ground displacements.

The Fourier spectrum of $\phi_i g$ can be evaluated by computing ϕ_i from the Fourier spectrum of translation, as in Eq. (4). To do this, it was assumed, for this illustration only, that the phase velocity $c(\omega) \approx 3.0$, 3.0, 3.0, 1.0, 0.3 and 0.1 km/s at $f = 10^{-3}$, 10^{-2}, 10^{-1}, 10^{-0}, 10^{1} and 10^{2} Hz. The spectra of $\ddot{\phi}_i r_i$ were approximated by multiplying the spectra of ϕ_i by $\omega^2 r_i$ (for SMA-1 accelerograph, $r_i \sim 8$ mm, Fig. 2). This gives Fourier amplitude spectra of $\phi_i g$ and $\ddot{\phi}_i r_i$ as shown in Fig. 5. It is seen that, for the example distance $R = 10$ km, for M larger then about 4, $\phi_i g$ goes to a constant as $\omega \to 0$. This can be explained by contributions to $\phi_i g$ from rotations leading to permanent ground displacement, as illustrated in Fig. 6. It is further seen that the contribution from $\ddot{\phi}_i r_i$ is large only for high frequencies, in this example with peaks near 10 Hz, and that the spectral amplitudes of $\ddot{\phi}_i r_i$ are larger than those of $\phi_i g$, in this example only, for frequencies higher than 10–20 Hz.

If it is assumed that permanent ground displacement is rising as a smooth ramp function from 0 to $d_{\max}$ over time interval T_0, then, the ground velocity will be a square pulse with width T_0 and amplitude $v_{\max} = d_{\max}/T_0$. The ground rotation will also be a square pulse with amplitude $v_{\max}/c(\omega)$ (see the last sentence of Section 2.3), with Fourier amplitude spectrum:

$$[v_{\max}/c(\omega)]T_0 \frac{\sin(\omega T_0/2)}{\omega T_0/2}.$$

This estimate of ground rotation implies that the Fourier amplitude of $\phi_i g \to [v_{\max}/c(\omega)]\, T_0\, g$ as $\omega \to 0$. Taking $v_{\max}$ from Table 1 and $c(\omega) = 3.0$ km/s would give spectral amplitudes at $R = 0$ and for $\omega \to 0$ in the range shown by the shaded bands in the lower left part of Fig. 6. The estimates in Table 1 were made independently of the long period Fourier amplitude spectra in the extension proposed by Trifunac [44]. To estimate $\phi_i g$ in Table 1, a range of values for $v_{\max}$ and T_0 versus magnitude was used [45]. Because of rapid attenuation of the permanent displacement field with increasing distance from the fault, for the $R = 10$ km examples in Fig. 5, it should be expected that only for $M \sim 7$ the spectra of $\phi_i g$ should be comparable to the estimates based on $v_{\max}$ in Table 1 ($= [v_{\max}/c(\omega)]T_0 g$), and for $M < 7$ the spectra of $\phi_i g$ should be proportionally smaller than those represented by $[v_{\max}/c(\omega)]T_0 g$, as shown in Fig. 6.

Fig. 7 illustrates the combined contribution of $\phi_i g$ and $\ddot{\phi}_i r_j$ to the response of a horizontal transducer, neglecting the contribution of cross-axis sensitivity and transducer

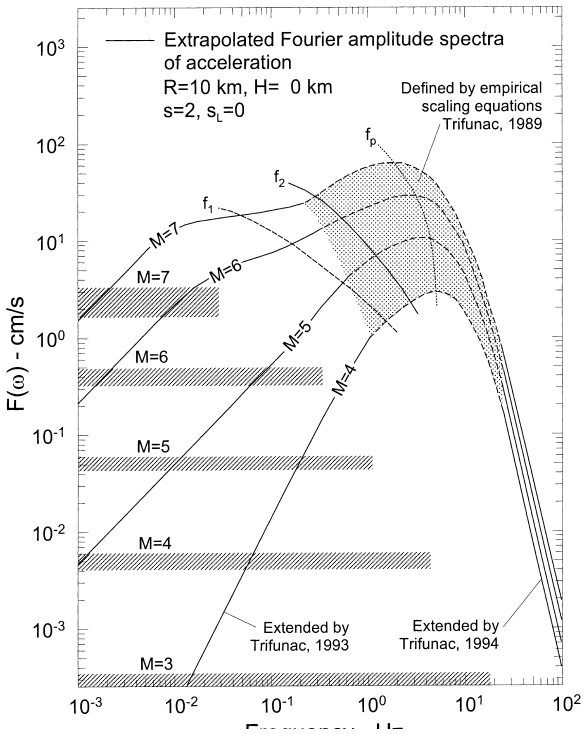

Fig. 6. Fourier amplitude spectra of ground acceleration (same as those in Fig. 5) and of normalized long period rotation $[v_{max}/c(\omega)]$ to g, shown by the horizontal gray shaded zones, associated with ground displacement that is a smooth ramp function with duration T_0 and permanent static displacement d_{max}. The lines labeled by f_1, f_2 and f_P show the location of the two long period corner frequencies [43,44] and of the peak spectral amplitudes.

misalignment. It is seen that for small r (here equal to 8 mm), the $\phi_i g$ terms are the main terms contributing to the modification of the transducer response. Fig. 7 also shows typical spectra of ambient noise for a 'noisy' and 'very noisy site'. The upper hatched area represents spectra of typical digitization noise in analog records (digitized manually or automatically) and the lower one of noise in PDR-1 and FBA transducers. The threshold recording levels for several strong motion accelerographs and recorders (SMA-1, QDR, PDR, Etna and K2) are also shown. It is seen that for the digital recorders, with resolution higher than 11–12 bits, the contribution of ground rocking cannot be ignored in computation of permanent displacements in the near-field.

Table 1
Range of values for peak ground velocity v_{max} (cm/s) and dislocation rise time $T_0(s)$ for magnitudes $M = 3$ to 8 (from Trifunac and Novikova [45]). The estimates of ϕg (cm/s^2) are shown in the last column

M	v_{max} (cm/s)	$T_0(s)$	ϕg (cm/s^2)
3	1–2	0.05	0.0033–0.0065
4	4–8	0.31	0.013–0.026
5	18–25	0.73	0.059–0.082
6	60–90	1.6	0.20–0.30
7	100–200	5.4	0.33–0.66
8	180–330	(26)	0.59–1.08

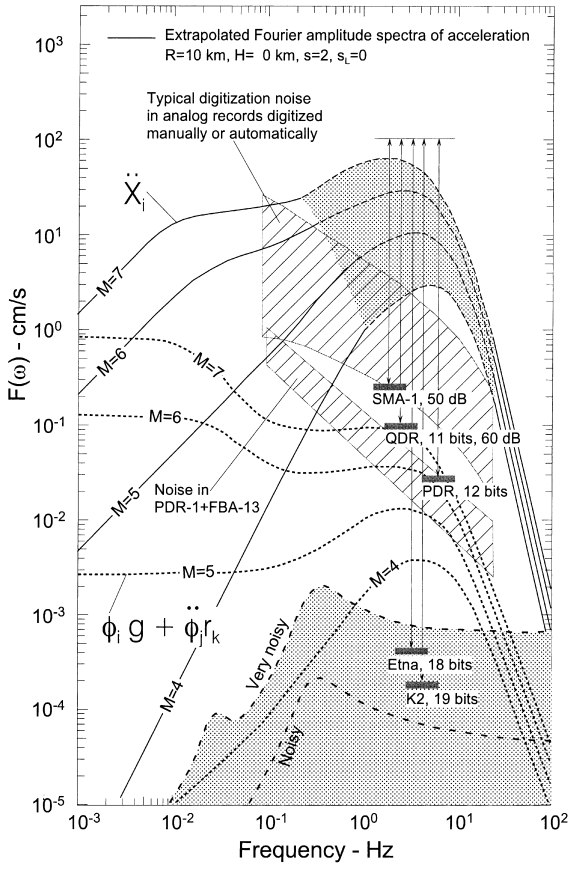

Fig. 7. Comparison of Fourier amplitude spectra of translation, $\ddot{X}_i$, with spectra of contributions from $\phi_i g + \ddot{\phi}_j r_k$, analog digitization noise, digital digitization noise (PDR), and microtremor and microseism noise.

3.2. Comparison of spectra of $\phi_i g$ and $\ddot{\phi}_i r_i$ with spectra of recording and processing noise

There are many factors contributing to the noise in digitized and processed data [1,6,7,14,46,47]. These factors depend on the type of transducer and its mechanical and electrical properties [23–25], the properties of the recording system (light sensitive paper, film, analog or digital tape, solid state memory, and the methods of data processing [2–5,29]. From the viewpoint of this paper, of interest is the total noise in the data distributed to users. Fig. 8 illustrates examples of this noise.

In Fig. 8, 'minimum digitization noise' describes the best quality data of acceleration recorded on paper or on film (enlarged up to four times) and digitized on hand-operated flat bed digitization tables. The bottom boundary of this zone corresponds to an average Fourier amplitude spectrum of digitization noise for duration of 15 s. The top boundary corresponds to the average plus one standard deviation of a noise spectrum for duration of 100 s [48]. Another type of digitization noise is associated with the automatic digitization system we introduced in 1978, based on an Optronics Drum Scanner [49]. It offered useful advantages over the old hand operated digitization: (1) the noise characteristics were

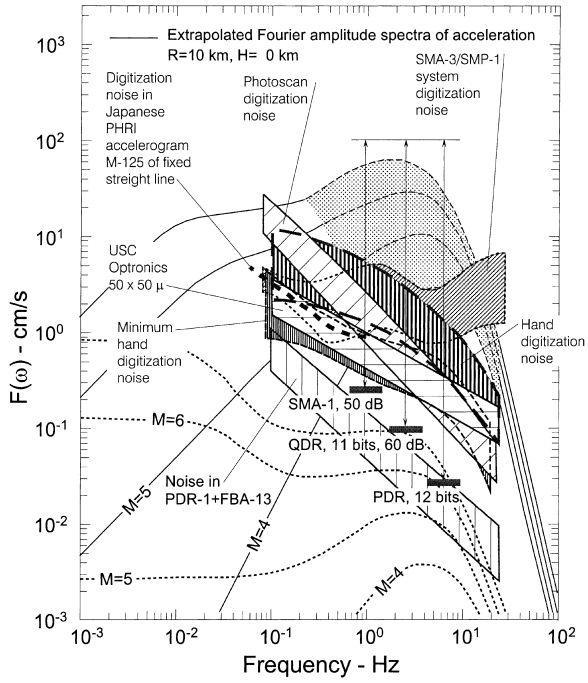

Fig. 8. Comparison of different noise spectra associated with different recording instruments and different methods of digitization.

reproducible and (2) the parallax errors were eliminated. SMA-3 was a multiple channel frequency modulated analog accelerograph that recorded signals onto a cassette tape. By SMP-1 playback, the analog data was converted into computer compatible nine-track magnetic tape. The digitizer was a 12-bit analog-to-digital converter. As shown in Fig. 8, this system had high noise amplitudes in the high frequency range. For comparison, we also show digitization noise in the Japanese PHRI accelerogram M-125, for signal duration of 12.5 s [46]. Fig. 8 also shows the average hand digitization noise (with similar shape but larger amplitudes than the 'minimum' hand digitization noise), and USC-Optronics (50×50 μ pixels) scanner noise, which is from the same family as the above 'Photoscan' digitization noise, but corresponds to more typical short records, usually shorter than 20 s. In Fig. 7, the above examples of noise amplitudes are combined into a broad zone. Consequently, this zone illustrates the range from the 'smallest' to the 'largest' digitization noise, representative of various methods of digitization of strong motion accelerograms mainly in the US and of most of the western US strong motion data recorded so far. Figs. 7 and 8 also show digitization noise amplitudes of digital PDR-1 recorder working with FBA-13 force balance type accelerograph [14].

Figs. 7 and 8 show that even for the most accurate digitization of analog records, the digitization noise is larger than the largest contributions from the spectra of $\phi_i g$ in Eq. (1) (assuming linear wave propagation for all strong motion amplitudes). Therefore, for linear wave motion (in the far-field), the contribution to 'translational' records coming from titling of accelerographs through angle ϕ_i can be neglected. For a 12 bit PDR-1 recorder, however, the effect of tilting can become comparable to and larger than the digitization noise and cannot be neglected. Finally, it should be clear from Fig. 7 that recording only translational accelerations with 18 and 19 bit recorders (e.g. Etna, or K2; both manufactured by Kinemetrics Inc.), without recording rotation is costly and not necessary. This can allow recording of smaller earthquakes and aftershocks, but cannot contribute to accurate calculation of permanent displacements of the ground and of structures in the near-field [50,51].

3.3. Estimates of $\phi_i g$ and $\ddot{\phi}_i r_i$ from synthetic translational and rotational time series

In the following, we illustrate the contribution to the forcing function from the translation, rocking and torsion of the instrument housing evaluated from synthetic time histories using the computer code SYNACC [40,41,52]. SYNACC is based on an earth model with parallel layers and produces Fourier spectrum compatible time histories of translational (radial and transverse) and rotational (rocking and torsion) components of motion. The latter are computed from the characteristics of the first several surface wave (Love and Rayleigh) modes allowable in the specified layered medium as well as P and S body waves, assuming small deformation (i.e. linear) wave propagation. Figs. 9 and 10 show time histories (part a) and Fourier spectra (part b) of the radial acceleration, rocking angle multiplied by g and torsional acceleration multiplied by $r(=0.8$ cm), for magnitude $M=6$, epicentral distances $R=5$ and 10 km, and for a site with physical properties specified in Table 2. These correspond to $\ddot{X}_1$, $\phi_2 g$ and $\ddot{\phi}_3 r_1$ in Eq. (1a) for the pendulum recording longitudinal motion. It is seen that the spectral

Table 2
Layer properties at the Westmoreland site in Imperial Valley [41,41] used to compute phase and group velocities for synthesis of $\ddot{X}_1$, ϕ_2 and $\ddot{\phi}_3$ in the examples shown in Figs. 9 and 10

Layer	Depth [km]	P-wave Velocity [km/s]	S-wave Velocity [km/s]	Density [gm/cm^3]
1	0.18	1.70	0.98	1.28
2	0.55	1.96	1.13	1.36
3	0.98	2.71	1.57	1.59
4	1.19	3.76	2.17	1.91
5	2.68	4.69	2.71	2.19
6	∞	6.40	3.70	2.71

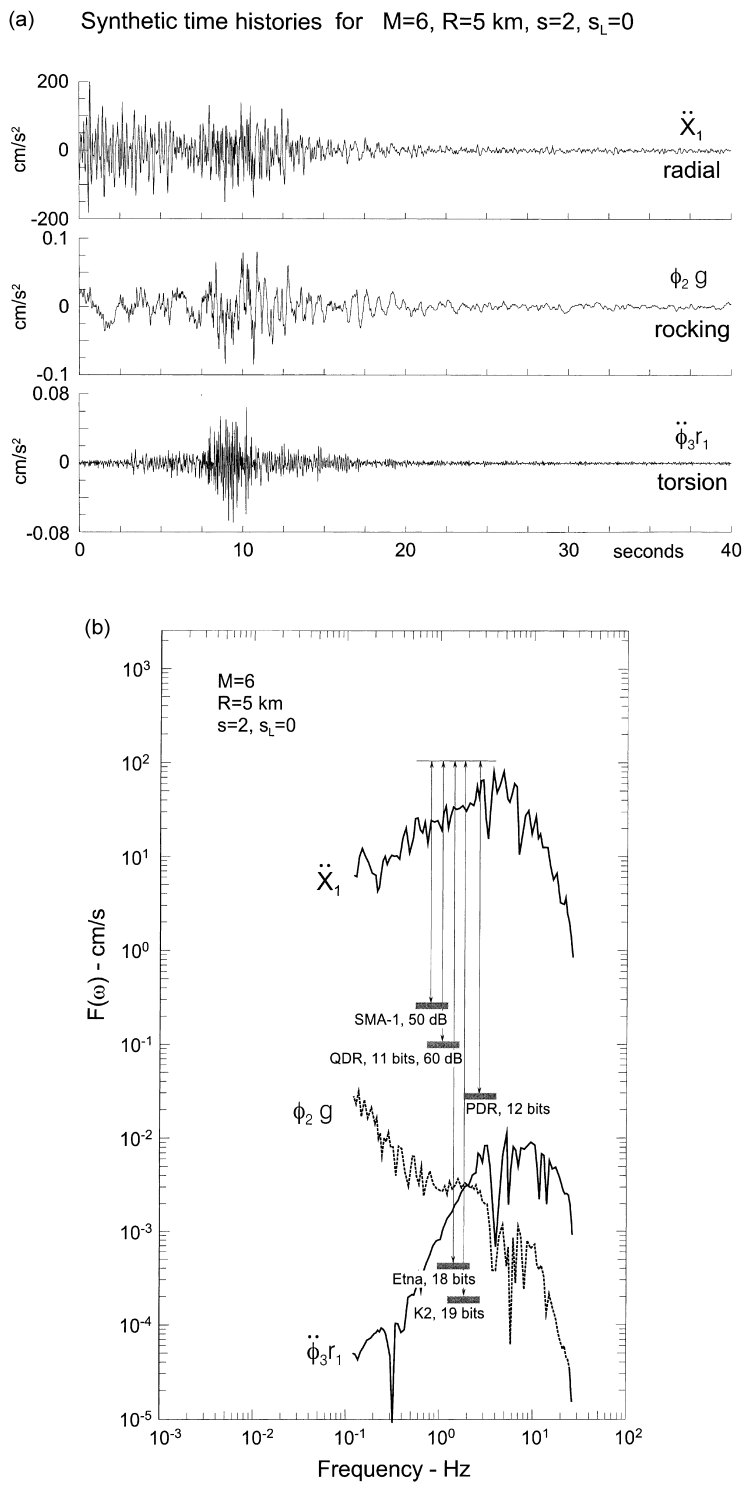

Fig. 9. Time histories (part a) and Fourier amplitude spectra (part b) of radial acceleration ($\ddot{X}_1$), normalized rocking angle (ϕ_2g) and normalized torsion ($\ddot{\phi}_3\, r_1$) computed by computer code SYNACC for a parallel layer model (Table 2) for magnitude $M = 6$, source to station distance $R = 5$ km, geologic site condition $s = 2$ (rock) and local soil condition $s_L = 0$ (rock soil).

amplitudes of the rotational terms are larger than the threshold recording amplitudes of Etna and K2 transducers, but below the noise levels for digitized film accelerograms.

The above estimates of angular displacements, velocities and accelerations are based on the linear theory of strong motion waves. During strong shaking in the near-field, the response of typical soil (average shear wave velocity ~300 m/s) begins to be non-linear when the peak ground velocities exceeds 15–20 cm/s, and large non-linear response occurs (fissures, lateral spreading, liquefaction,

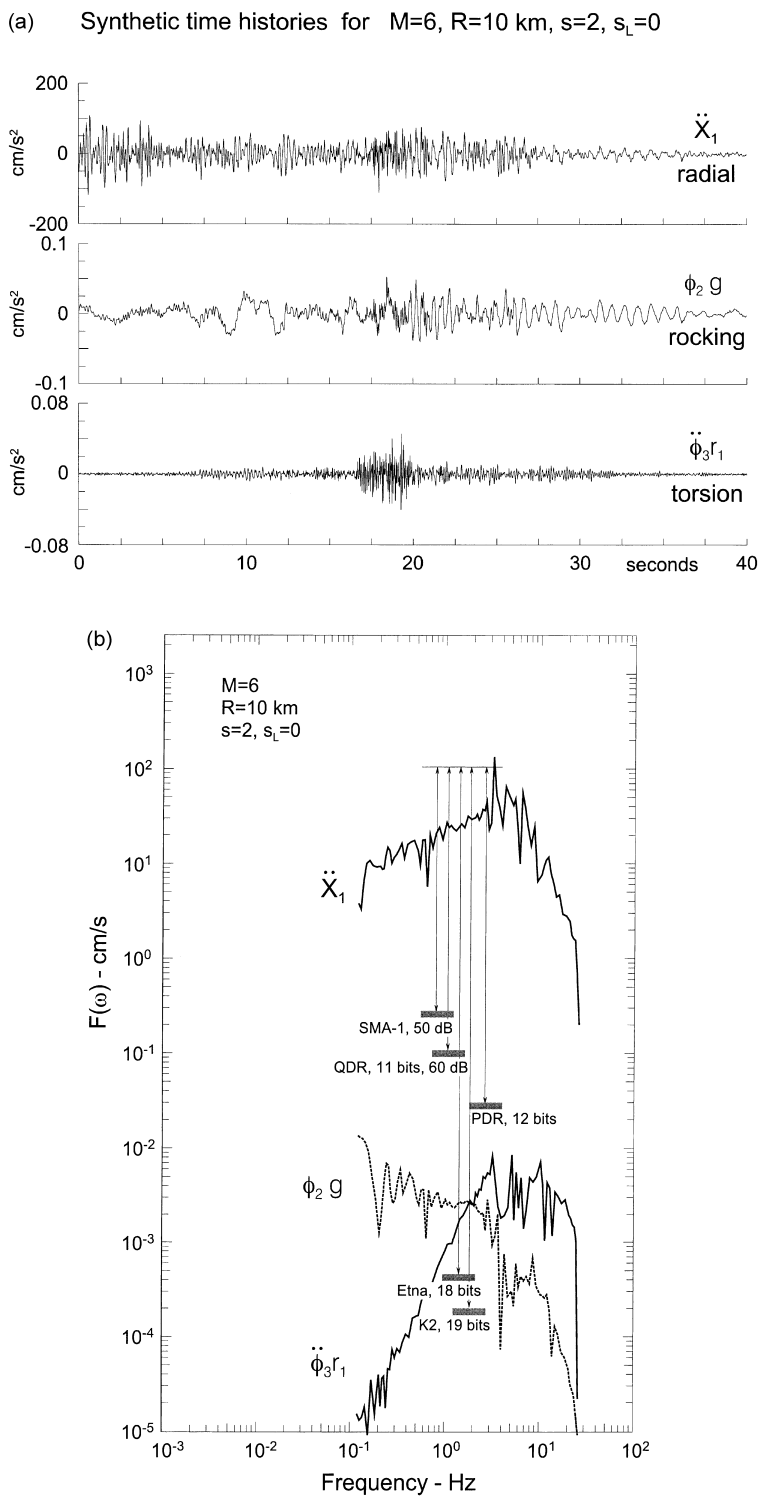

Fig. 10. Same as Fig. 9 but for source to site distance $R = 10$ km.

settlement, …) when peak ground velocity exceeds about 50 cm/s [53–60]. Non-linear site response will contribute additional and much larger rotations and tilts, beyond those associated with linear estimates of permanent ground deformation and wave propagation. These additional non-linear motions cannot be described in general, because those will depend on the details of the site properties and on the time history of the excitation. Consequently, the contributions to the forcing functions in Eq. (1) associated with tilting and angular accelerations, as described in Fig. 7, can be considered only to represent smoothed lower bound of the total rotation and angular acceleration.

4. Discussion and conclusions

The main message of this paper is that it is not possible to compute accurately and reliably permanent displacements of the ground (or of structures) without simultaneously recording rotations during strong motion. This message is not new. It was discussed by Graizer, 10–15 years ago in a series of articles [17,34,61] and in the monograph entitled 'True ground displacements in epicentral zone' [12]. Unfortunately this important work appears to be ignored by most of the recently published papers.

Recording rotations is essential for complete specification of the response of the horizontal acceleration transducers (L and T transducers, Fig. 3 and Eqs. 1(a) and (b), and cannot be neglected for digital recorders with resolution grater than about 12 bits (Fig. 7). Only the linearized form of the differential equation of the transducer recording vertical acceleration is not affected by strong motion tilting. All transducers however (vertical and horizontal) are affected by the angular accelerations, but the effect is relatively small, either because r is small (Fig. 5), or because $r = 0$ (depending on the details of the transducer design). The cross-axis sensitivity ($X_i\ \alpha_j$ terms in Eq. (1)) and misalignment terms (not included in Eq. (1)) have been analyzed in some detail [25,26,31] and therefore are not discussed in this paper. The cross-axis sensitivity errors are such that they add sharp pulses to the record of translational acceleration. In time these pulses coincide with the largest peaks of strong motion acceleration. After integrating twice, these peaks contribute to large 'permanent displacements', which, after all motion has stopped, will 'grow' parabolically with time.

In the absence of recorded rotational components of strong motion, in this paper, the spectral amplitudes of rotation were estimated from average Fourier spectra of translations and from synthetically computed accelerograms, based on linear wave propagation theory in layered soil and sediments. It is expected that such estimates are approximately correct in the far-field. In the near-filed, where the soil may experience non-linear response, and in structures undergoing damage [62,63], the rotational components of strong motion are expected to be larger than the linear estimates, and the need to include them in the analysis of motion is even more apparent.

We illustrated the nature of the rocking and torsional motions for earthquake magnitude $M = 6$, $R = 5$ and 10 km hypocentral distance, and showed that, for a typical 12 bit recorder, the contributions to the forcing function in the transducer equation of motion from the rotational motions are comparable to those of the recording noise. Similar analysis can be performed for other magnitudes and epicentral distances and for recorders with different resolution and overall recording noise characteristics, and can be used to select the optimal number of bits for a six component (three translations and three rotations) strong motion recorder.

The development and field deployment of instruments capable of recording all six components of strong motion, with resolution exceeding about 20 bits, will contribute to the next quantum jump in recording, interpretation and understanding of the near-field strong motion phenomena, and of permanent non-linear and damaging response of structures [13,62,63]. Until this is realized, the 'standard' data processing methods should continue to work with band-limited acceleration, velocity and displacement. As the recording and digitization noise becomes smaller, this band will eventually broaden towards zero frequencies, and the computed velocities and displacements will converge to their true values that include permanent displacement. In the meantime, the available resources for recording strong motion should be optimized, avoiding excessive expenditures on high resolution and high dynamic range recorders where such high performance in recording translations only is not justified. Finally, it is hoped that the researchers who claim that 'it is possible to recover the long period information from near-field strong motion accelerographs by an appropriate processing scheme,… using the proposed algorithm' will recognize that permanent ground displacement cannot be computed without the knowledge of the rotational components of strong motion, especially in the near-field of moderate and strong earthquakes where the response of the ground and structures may be non-linear.

Recording angular components of strong motion will open innumerable new possibilities in engineering and seismological studies, especially in the near-field and in studies of non-linear soil and structural response. Measured rotations will help identify and separate P and SV waves from SH components and Love from Rayleigh waves. Recording rotations near and on foundations of structures will help separate (from the total motions), and better identify the motions associated with soil–structure-interaction. Recorded rotational data will provide for the first time detailed picture of the relative interstory drift, by enabling us to separate the contributions of rocking from those of relative translational deformation. This will in turn help determine more realistic estimates of P-delta effects in full-scale structures. Simultaneous recording of all six components of motion will enable computations of permanent displacement in structures, soils and in the near field of ground near shallow earthquake faults. This enumeration could go on, but the benefits of recording all six components of motion are overwhelming, and should be obvious.

Acknowledgements

We thank Dr. Vladimir Graizer for sharing with us copies of his early contributions to this subject and for his constructive comments and suggestions on how to improve this paper.

References

[1] Trifunac MD, Udwadia FE, Brady AG. High frequency errors and instrument corrections of strong-motion accelerogram. Earthq Engrg Res Lab EERL 71-05, Calif Inst of Tech, Pasadena, California, 1971.

[2] Trifunac MD. Zero baseline correction of strong-motion accelerograms. Bull Seism Soc Amer 1971;61:1201–11.
[3] Trifunac MD. A note on correction of strong-motion accelerograms for instrument response. Bull Seism Soc Amer 1972;62:401–9.
[4] Trifunac MD, Lee VW. Routine computer processing of strong-motion accelerograms. Earthquake Eng Res Lab, EERL 73-03, Calif Inst of Tech, Pasadena, California, 1973.
[5] Trifunac MD, Lee VW. A note on the accuracy of computed ground displacement from strong-motion accelerograms. Bull Seism Soc Amer 1974;64:1209–19.
[6] Amini A, Trifunac MD, Nigbor RL. A note on the noise amplitudes in some strong motion accelerographs. Soil Dynamics and Earthquake Eng 1987;6(3):180–5.
[7] Lee VW, Trifunac MD, Amini A. Noise in earthquake accelerograms. ASCE, EMD 1982;108:1121–9.
[8] Trifunac MD. A three-dimensional dislocation model for the San Fernando, California, Earthquake of February 9, 1987. Bull Seism Soc Amer 1974;64:149–72.
[9] Trifunac MD, Udwadia FE. Parkfield, California, earthquake of June 27, 1966: a three-dimensional moving dislocation. Bull Seism Soc Amer 1974;64:511–33.
[10] Haskell NA. Elastic displacements in the near-field of a propagating fault. Bull Seism Soc Amer 1969;59:865–908.
[11] Bogdanov VE, Graizer VM. The determination of the residual displacement of the ground from the seismogram. Reports of the Academy of Sciences of the USSR 1976;229:59–62.
[12] Graizer VM. Istinoye dvizheniye pochvi v epicentralnoy zone. Akadamia Nauk, SSSR, Moscow: Institute of Earth Physics, 1984.
[13] Trifunac MD, Todorovska MI. Evolution of accelerographs, data processing, strong motion arrays, and amplitude and spatial resolution in recording strong earthquake motion. Soil Dynamics and Earthquake Engineering 2001;21:in press.
[14] Iwan WD, Moser MA, Peng C-Y. Some observations on strong-motion earthquake measurement using digital accelerograph. Bull Seism Soc Amer 1985;75(5):1225–46.
[15] Wang L-J, Gu Q, Iwan WD. A collection of processed near-field earthquake accelerograms with response and drift spectra. Earthquake Eng Res Lab EERL 96-15, Calif Inst of Tech, Pasadena, California, 1996.
[16] Chung J-K, Shin T-C. Implications of rupture process from the displacement distribution of strong motions recorded during the 21 September 1999 Chi-Chi, Taiwan Earthquake. Terestrial, Atmospheric and Oceanic Sciences 1999;10(4):777–86.
[17] Griazer VM. On inertial seismometry. Izvestiya, Earth Physics, Akademia Nauk, SSSR 1989;25(1):26–29.
[18] Carder DS. Vibrational observations, Chapter 5. Earthquake investigations in California 1934–1935. Special Publication No. 201, US Dept. of Commerce, Coast and Geodetic Survey, 1936. p. 49–106.
[19] Golitsyn BB. Lektsii po Seysmometrii (Lectures on Seismometry), Sib. Izd. Rossiyskoy Akad. Nauk, Moskva, 1912.
[20] Heck NH, McComb HE, Ulrich FP. Strong-motion program and tiltmeters, Chapter 2. Earthquake investigations in California 1934–1935. Special Publication No. 201, US Dept. of Commerce, Coast and Geodetic Survey, 1936. p. 4–30.
[21] Hudson DE. Ground motion measurements, Chapter 6. In: Wiegel R, editor. Earthquake engineering. Englewood Cliffs, NJ: Prentice-Hall, 1970. p. 107–25.
[22] Hudson DE. Dynamic tests of full-scale, Chapter 7. In: Wiegel R, editor. Earthquake engineering. Englewood Cliffs, NJ: Prentice-Hall, 1970. p. 127–49.
[23] Amini A, Trifunac MD. Analysis of a feedback transducer. Dept of Civil Eng Rep No. 83-03, University Southern California, Los Angeles, California, 1983.
[24] Amini A, Trifunac MD. Analysis of force balance accelerometer. Soil Dynamics and Earthquake Eng 1985;4(2):83–90.
[25] Todorovska MI. Cross-axis sensitivity of accelerographs with pendulum like transducers—mathematical model and the inverse problem. Earthquake Engrg and Struct Dynam 1998;27(10):1031–51.
[26] Wong HL, Trifunac MD. Effects of cross-axis sensitivity and misalignment on response of mechanical–optical accelerographs. Bull Seism Soc Amer 1977;67:929–56.
[27] Graizer VM. On the determination of displacement from strong-motion accelerograms. Proceedings of the Seventh World Conference on Earthquake Eng, Istanbul. Vol. 2, 1980. p. 391–94.
[28] Aki K, Richards P. Quantitative seismology. San Francisco: W.H. Freeman, 1980.
[29] Lee VW, Trifunac MD. Automatic digitization and processing of accelerograms using personal computers. Dept of Civil Eng, Rep. No. 90-03, University of Southern California, Los Angeles, California, 1990.
[30] Novikova EI, M D. Trifunac digital instrument response correction for the force balance accelerometer. Earthquake Spectra 1992;8(3):429–42.
[31] Todorovska MI, Novikova EI, Trifunac MD, Ivanovic SS. Advanced accelerograph calibration of the Los Angeles strong motion array. Earthquake Eng and Structural Dynamics 1998;27(10):1053–68.
[32] Farrell WE. A gyroscopic seismometer: measurements during the Borrego Earthquake. Bull Seism Soc Amer 1969;59(3):1239–45.
[33] Nigbor RL. Six-degree-of-freedom ground-motion measurement. Bull Seism Soc Amer 1994;84(5):1665–9.
[34] Griazer VM. Ob izmerenii naklona zemnoi poverhnosti vblizi epicentra vzriva. Dokladi Akademii Nauk S.S.S.R., Geofizika 1989;305(2):314–8.
[35] Gupta VK, Trifunac MD. Response of multistoried buildings to ground translation and torsion during earthquakes. European Earthquake Eng 1990;IV(1):34–42.
[36] Gupta VK, Trifunac MD. Effects of ground rocking on dynamics response of multi-storied buildings during earthquakes. Structural Eng/Earthquake Eng, JSCE 1991;8(2):43–50.
[37] Trifunac MD. Response envelope spectrum and interpretation of strong earthquake ground motion. Bull Seism Soc Amer 1971;61:343–56.
[38] Trifunac MD. A method for synthesizing realistic strong ground motion. Bull Seism Soc Amer 1971;61:1739–53.
[39] Trifunac MD. A note on rotational components of earthquake motions for incident body waves. Soil Dynamics and Earthquake Eng 1982;1(1):11–19.
[40] Lee VW, Trifunac MD. Torsional accelerograms. Soil Dynamics and Earthquake Eng 1985;4(3):132–9.
[41] Lee VW, Trifunac MD. Rocking strong earthquake accelerations. Soil Dynamics and Earthquake Eng 1987;6(2):75–89.
[42] Trifunac MD. Dependence of Fourier spectrum amplitudes of recorded strong earthquake accelerations on magnitude, local soil conditions and on depth of sediments. Earthquake Eng and Structural Dynamics 1989;18(7):999–1016.
[43] Trifunac MD. Q and high frequency strong motion spectra. Soil Dynamics and Earthquake Eng 1994;13(3):149–61.
[44] Trifunac MD. Long period Fourier amplitude spectra of strong motion acceleration. Soil Dynamics and Earthquake Eng 1993;12(6):363–82.
[45] Trifunac MD, Novikova EI. Duration of earthquake fault motion in California. Earthquake Eng and Structural Dynamics 1995;24(6):781–99.
[46] Crouse CB. Data Processing, Proc Golden Anniversary Workshop on Strong Motion Seismometry, March 30–31, University of Southern California, Los Angeles, California, 1983.
[47] Trifunac MD, Udwadia FE, Brady AG. Analysis of errors in digitized strong-motion accelerograms. Bull Seism Soc Amer 1973;63:157–87.
[48] Trifunac MD. Preliminary empirical model for scaling Fourier amplitude spectra of strong ground acceleration in terms of earthquake magnitude, source to station distance and recording site conditions. Bull Seism Soc Amer 1976;66:1343–73.
[49] Trifunac MD, Lee VW. Automatic digitization and processing of strong-motion accelerograms, Parts I and II. Dept. of Civil Eng.,

Report No. 79-15, University of Southern California, Los Angeles, California, 1979.

[50] Finn WEL. Permanent deformations in ground and earth structures during earthquakes. Proceedings of the Ninth World Conference on Earthquake Engineering, Tokyo-Kyoto 1988;VIII:201–12.

[51] Hamada M, Saito K. Earthquake damage by liquefaction-induced permanent ground displacement. Proceedings of the Ninth World Conference on Earthquake Engineering, Tokyo-Kyoto 1988; VIII:213–8.

[52] Wong HL, Trifunac MD. Generation of artificial strong motion accelerograms. Earthquake Eng and Structural Dynamics 1979;7(6):509–52.

[53] Trifunac MD, Todorovska MI. Non-linear soil responses—1994 Northridge California Earthquake. J Geotechnical Eng, ASCE 1996;122(9):725–35.

[54] Trifunac MD, Todorovska MI. Northridge, California, earthquake of 17 January 1994: density of pipe breaks and surface strains. Soil Dynam and Earthquake Engrg 1997;16(3):193–207.

[55] Trifunac MD, Todorovska MI. Non-linear soil response as a natural passive isolation mechanism—the 1994 Northridge, California earthquake. Soil Dynam and Earthquake Engrg 1998;17(1):41–51.

[56] Trifunac MD, Todorovska MI. Damage distribution during the 1994 Northridge, California, earthquake relative to generalized categories of surficial geology. Soil Dynamics and Earthquake Eng 1998;17(4):239–53.

[57] Trifunac MD, Todorovska MI. Amplification of strong ground motion and damage patterns during the 1994 Northridge, California earthquake. Proceedings of the ASCE Specialty Conference on Geotechnical Earthquake Engineering and Soil Dynamics, Seattle, Washington. Geotechnical Special Publ. No. 75, ASCE, 1. 1998. p. 714–25.

[58] Trifunac MD, Todorovska MI. Recording and interpreting earthquake response of full scale structures. NATO Advanced Research Workshop on Strong Motion Instrumentation for Civil Engrg Structures, June 2–5, Istanbul, Kluwer (in press), 1999.

[59] Trifunac MD, Todorovska MI. Reduction of structural damage by non-linear soil response. J Structural Eng, ASCE 1999;125(1):89–97.

[60] Trifunac MD, Todorovska MI. Can aftershock studies predict site amplification factors—Northridge, California, earthquake of 17 January 1994. Soil Dynamics and Earthquake Eng 2000; 19:253–67.

[61] Graizer VM. Metodi Inercialnoi Seismometrii. Dokladi Akademii Nauk SSSR, Fizika Zemli 1991;1:72–87.

[62] Trifunac MD, Ivanovic SS, Todorovska MI. Apparent periods of a building. Part I: Fourier analysis. J of Structural Eng, ASCE 2001 (in press).

[63] Trifunac MD, Ivanovic SS, Todorovska MI. Apparent periods of a building. Part II: time-frequency analysis. J of Structural Engineering, ASCE 2001 (in press).